Science Advances
AAAS

advances.sciencemag.org/cgi/content/full/6/3/eaay7243/DC1

Supplementary Materials for

Biophysical and biomolecular interactions of malaria-infected erythrocytes in engineered human capillaries

Christopher Arakawa, Celina Gunnarsson, Caitlin Howard, Maria Bernabeu, Kiet Phong, Eric Yang, Cole A. DeForest*, Joseph D. Smith*, Ying Zheng*

*Corresponding author. Email: yingzy@uw.edu (Y.Z.); joe.smith@seattlechildrens.org (J.D.S.); profcole@uw.edu (C.A.D.)

Published 17 January 2020, *Sci. Adv.* **6**, eaay7243 (2020)
DOI: 10.1126/sciadv.aay7243

The PDF file includes:

Other Supplementary Material for this manuscript includes the following:

(available at advances.sciencemag.org/cgi/content/full/6/3/eaay7243/DC1)

Movie S4 (.mp4 format). Representative video of normal RBCs stretching through capillaries (diameter, ~10 μm) when perfused at the single-cell scale.
Movie S5 (.mp4 format). Representative video of normal RBCs tumbling through capillaries (diameter, ~10 μm) when perfused at the single-cell scale.
Movie S6 (.mp4 format). Representative video of 2G2 IRBCs tumbling through capillaries (diameter, ~10 μm) when perfused at the single-cell scale.
Movie S7 (.mp4 format). Representative video of normal RBCs perfused through the capillaries at physiological hematocrit with no cell accumulation in the lumen.
Movie S8 (.mp4 format). Representative video of IT4VAR19 IRBCs perfused through the capillaries at physiological hematocrit accumulating a significant amount and blocking the capillary flow.
Movie S9 (.mp4 format). Representative video of trypsinized IT4VAR19 perfused through the capillaries showing a significant decrease in cell accumulation and not blocking the capillary flow.
Movie S10 (.mp4 format). Representative video of 2G2 IRBCs perfused through the capillaries at physiological hematocrit accumulating at postcapillary regions but not blocking the capillary flow.

SUPPLEMENTARY MATERIALS AND METHODS

Cell culture: HUVECs (Lonza) were cultured according to the manufacturer's guidelines using EBM Basal Medium supplemented with EGM Endothelial Cell Growth Medium SingleQuots Supplements (Lonza). For all experiments HUVECs were used between passage 3 and 7.

Fabrication of arteriole and venule sized microchannels. Lithography and injection molding-based techniques are used to define conduits and networks in collagen gel(*31*). Two major steps are involved:

Step 1: PDMS micropatterned stamp fabrication. Geometry of two parallel microchannels (diameter of 200 μm) with independent inlets and outlets was designed using computer-aided design software and fabricated using a standard photolithography process(*31*). Briefly, a silicon wafer was spin-coated with SU-8 photoresist (Microchem), soft-baked at 65ºC for 7 min, at 95ºC for 1 hr, and then cooled to 20ºC. A negative chrome photomask was placed on the spin-coated wafer, and the wafer was exposed to UV light (λ = 365 nm), then baked at 65 ºC for 19 min, at 95 ºC for 1 hr, and then cooled to 20ºC. The exposed wafer was submerged in SU-8 developer and then cleaned with isopropyl alcohol and evaporation silanized overnight with trichloro(3,3,3-trifluoropropyl)silane (Sigma). Liquid PDMS with crosslinker (Dow Corning) was mixed at 10:1 ratio and poured over the wafer pattern, cured at 65°C overnight, then peeled off the mold to generate a micropatterned stamp for vessel fabrication.

Step 2: Engineering two main arteriole or venule-sized microchannels in collagen gel. Type I collagen was isolated from rat tails, lyophilized and resuspended to a stock concentration of 15 mg/ml in 0.1% acetic acid following a standard protocol (*61*), then diluted with cell culture media and neutralized to 7.5 mg/ml on ice before microvessel fabrication. The two main channels within each microvessel device (lumenal diameters: ~200 μm) were fabricated using soft lithography and injection molding as previously described(*31*). Briefly, collagen was injected into a PEI/glutaraldehyde–treated Plexiglas housing top half that formed the negative impression of a microvessel network along with a PDMS stamp. Inlet and outlet ports were formed by inserting stainless steel dowel pins before injecting the collagen. The Plexiglas bottom half consisted of a flat layer of collagen compressed by a flat PDMS surface that was gelled on

top of a standard coverslip. The collagen was allowed to gel for 30 min at 37 °C. After gelation, the PDMS pieces were removed and the two halves were brought together to seal the microchannel conduits. Culture medium was then added to the individual inlet reservoirs and incubated for 2 hr before cell seeding or preparation for multi-photon ablation to generate capillary-sized channels between two main channels.

Multi-photon ablation for the generation of acellular arteriole-capillary-venule unit. Multiphoton photoablation was performed in collagen gel in the two parallel microchannel devices using a Mai Tai DeepSee Ti:S laser (maximum power 2.57W) coupled with an Olympus FV1000 MPE BX61 microscope fitted with a water-immersion objective lens (25x, NA = 1.05). Microchannels and surrounding collagen regions were first identified by taking advantage of second-harmonic generation signals produced by collagen microfibers at excitation wavelength λ_{ex} = 860 nm and detection wavelength $\lambda_{detector}$ = 420-460 nm. Individual capillary-sized channels were designed within the collagen matrix by designating 3D regions of interest using the Olympus Fluoview software then ablated by laser rastering (λ = 800 nm, I = 100%, pixel dwell time = 2 μs, 10-15 line repeat scans). Laser scanning in the X, Y, and Z dimensions were performed at ~1 μm step sizes. After the ablation, fluorescent microbeads at diameter of 0.22 μm were perfused from one side of main channels across the newly created microchannels to the other side at a pressure drop of 1 cmH_2O for 10 mins, followed by imaging for evaluation of perfusability (fig. S1).

Endothelializing arteriole-capillary-venule unit: We investigated two different procedures to form the endothelialized ACV units: i). direct cell seeding of acellular channels and ii). endothelial cell in-growth after photoablation (fig. S3). In the first approach, the acellular ACV unit is first fabricated by photoablation, followed by seeding cells into the fully acellular device through the inlets of the two main parallel channels with 10 μL injections of HUVECs at a density of 8 x 10^6 cells/mL. The seeded cells were found to start attach in the microchannels 5 mins after seeding, and all inlets and outlets were filled with media to the same height to allow firm cell attachment and sufficient media access overnight. Once the cells were attached, the devices were cultured under gravity-driven flow across the capillaries between two main channels for 7 days. To create a gravity-flow, 200 μL and 180 μL of culture media is placed in

the two main channel inlets, to set the initial pressure drop at approximately 1 cmH_2O, leading to a peak velocity of approximately 1 mm per sec across the ACV unit between the two main channels. The pressure drop was reset every 12 hrs to maintain flow in capillary regions.

In the second approach, the two main microchannels were first seeded with HUVECs at a density of 8 x 10^6 cells/mL and cultured for 3 days to form robust endothelialized lumen. Multiphoton photoablation was then performed to create capillary sized microchannel void spaces within the collagen scaffold between the lumenal wall of the two main vessels and ablate endothelial cells at the two end connections. For Fig. 1B-E and fig. S2, microchannels at sizes of 10 or 20 μm were fabricated as 2×2 arrays with distances of 5, 10 and 20 μm to determine the minimal distance between two capillaries and minimal diameter for each capillary to develop continuous endothelium with robustness and patency. For Fig. 1F and onwards, hourglass shaped microchannels were ablated as individual channels with 100 μm apart from each other. The hourglass shape includes a precapillary arteriole and a postcapillary venule mimicking vessels with constant width (width w = 40 μm, length l = 80 μm), which were connected to a capillary-sized region (w = 5 μm, l = 80 μm by two flanking narrowing/expanding transition regions (w = 40 μm to 5 μm, l = 105 μm). Cellular and collagen ablation was confirmed by imaging identical areas after ablation using transmitted light and by second harmonic generation of collagen microfibers via conventional multiphoton microscopy. The ablated vessels were then cultured for an additional 4 days to allow for endothelial cell ingrowth. The culture was maintained at the same pressure drop as the first approach and replenished twice a day with fresh culture media.

Immunofluorescence microscopy. To visualize the endothelial cell junctions and vessel structures, at designated time, the ACV vessel units were fixed *in situ* by perfusing 3.7% paraformaldehyde through inlets of one main microvessel inlets, across the capillaries, and into the outlets of the second microvessels. After three washes with PBS using gravity-based perfusion, the ACV unit was then incubated in Background Buster (Innovex) for 30 mins and blocking buffer (2% bovine serum albumin, 0.1% Triton-X in PBS) for 1 hr. Blocked microvessels were incubated overnight in primary antibodies (1:100, rabbit anti-VE-Cadherin, ab33168; 1:500, FITC-conjugated sheep anti-von Willebrand Factor (VWF), ab8822; Abcam) diluted in blocking buffer, washed, then incubated with secondary antibodies (1:200 goat anti-

rabbit Alexa Fluor 568, A11031; goat anti-rabbit Alexa Fluor 647, A21244; and goat anti-mouse Alexa Fluor 647, A21235; Invitrogen) for 1 hr. Stained microvessels were imaged using a Nikon A1R confocal microscope, and image stacks were acquired with a ~3 μm z-step distance between optical slices. Cross-sections and projections were produced from z-stacks using ImageJ software.

Histological analysis *(Cryosectioning and staining).* Fixed microvessels were removed from their acrylic housing and equilibrated in optical cutting temperature (OCT) compound (Thermofisher) overnight at 4°C before transferring into fresh OCT and freezing in a 100% ethanol and dry ice slurry. Frozen blocks were sectioned at 10 μm thickness on a Leica CM1850 cryostat. Sections were stained with Hematoxylin and Eosin (H&E), then viewed on a light microscope. Additional sections were stained for collagen IV (1:100, Abcam, ab6586) by Abidin-Biotin Complex (ABC) immunoperoxidase method using an ABC-HRP kit (Vectorlabs), then developed with SIGMAFAST DAB (Sigma-Aldrich).

RBC isolation. Fresh normal red blood cells were used within 3 days of isolation for experiments. Fresh whole blood was drawn from consenting healthy donors, who were nonsmokers and drug and aspirin free for at least three days prior to blood donation, under protocols approved by the Institutional Review Board of the University of Washington. RBCs were isolated from whole blood by centrifugation on a Ficoll-Paque (Sigma-Aldrich; specific gravity = 1.077 g/mL) gradient at 1500 rpm for 20 mins. The platelet-rich plasma and buffy coat were removed, and the packed RBC volume was washed three times in Dulbecco's phosphate buffered saline solution (DPBS) buffer. Purity of the RBC preparation was assessed with a thick blood smear, which was fixed in 100% methanol, stained with 1x Field's stain and visualized at 40X to confirm the absence of white blood cells.

Parasite culture. *P. falciparum* parasite lines were cultured using anonymized human O+ type red blood cells (Valley Biomedical) in RPMI-1640 (Gibco) supplemented with 10% human type A+ serum in a gas mixture of 90% N_2, 5% CO_2 and 5% O_2. The knobless parasite line 2G2 was previously derived by lack of gelatin floatation followed by limited dilution cloning (*40*), while the IT4VAR19 line was generated after repeatedly panning on transformed human brain

microvascular endothelial cells (THBMEC) followed by limited clonal dilution.(*59, 60*) Mature-stage infected red blood cells were enriched to 60-90% parasitemia by magnetic separation (MACS Cell Separator, LD columns, Miltenyi Biotech) prior to perfusion for single cell and population dynamics experiments. Both parasite lines predominantly express a single *var* gene and were derived from the IT4/FCR3 parasite genotype.

Determination of var transcription by qRT-PCR. Because *var* gene expression switches over time, the *var* transcription profile of the parasite lines was regularly monitored by qRT-PCR with a specific set of primers specific to the IT4 *var* gene repertoire. RNA was obtained from sorbitol-synchronized ring-stage parasites (~8-12h post-invasion), extracted in Trizol LS (Invitrogen) and reversed transcribed using random hexamers and MultiScribe reverse transcriptase (Thermo Fisher). qRT-PCR reactions were performed using Power-SYBR green Master Mix (Thermo Fisher) in an ABI Prism 7500 Thermal Cycler following published amplification conditions. Relative transcription of *var* genes was determined by normalization to the control housekeeping gene seryl-tRNA-synthetase (STS; PF07_0073) and the level of expression was represented as transcript units (TU) and calculated as $TU=2^{(-\Delta CT)}$.

Ultrastructural analysis. Microfluidic vascular networks were examined under transmission electron microscopy as described previously (*62*). Briefly, networks were fixed by half-strength Karnovsky's solution (2% paraformaldehyde/2.5% glutaraldehyde in 0.2 M cacodylate buffer) for 20 min followed by full immersion following disassembly in the same fixative solution for several days. Next, samples were post-fixed with 2% OsO_4 in 0.2 M cacodylate buffer, then dehydrated using immersions in graded solutions of ethanol, then propylene oxide (PO), before 1:1 PO/Epon 812 (Ted Pella Inc., Redding, CA) immersion overnight. Epon blocks were cured for 48 h at 60 °C then sectioned into ultrathin sections (70 nm) and placed onto grids. Grids were stained with uranyl acetate for 2 h and lead citrate for 5 min, then imaged using a JEOL JEM-1400 Transmission Electron Microscope (JEOL Ltd., Japan) using a typical acceleration voltage around 100 kV. Images were acquired with a Gatan Ultrascan 1000XP camera (Gatan, Inc., Pleasanton, CA).

Flow analysis. The velocity profile of flow through the capillary region, as shown in Fig. 3B was estimated qualitatively as steady Newtonian flow with the change of diameter along the capillaries. Based on the mass conservation, the average velocity $\langle U \rangle$ in the narrow region with diameter of 10 μm is 16 fold higher than that in the entrance or exit region of capillaries with diameter of 40 μm. The velocity profile is estimated to be parabolic function of vessel diameter r based on the Poiseuille flow: $u(r) = 2\langle U \rangle \left(1 - \frac{r^2}{R^2}\right)$ where R is the capillary diameter, and $r = R$ at the vessel wall, and $r = 0$ at vessel center. Though the flow of RBCs through capillaries is highly non-Newtonian, we expect no significant difference for the trend of velocity profile and changes of the average velocity along the longitudinal axis of the capillaries.

SUPPLEMENTARY FIGURES:

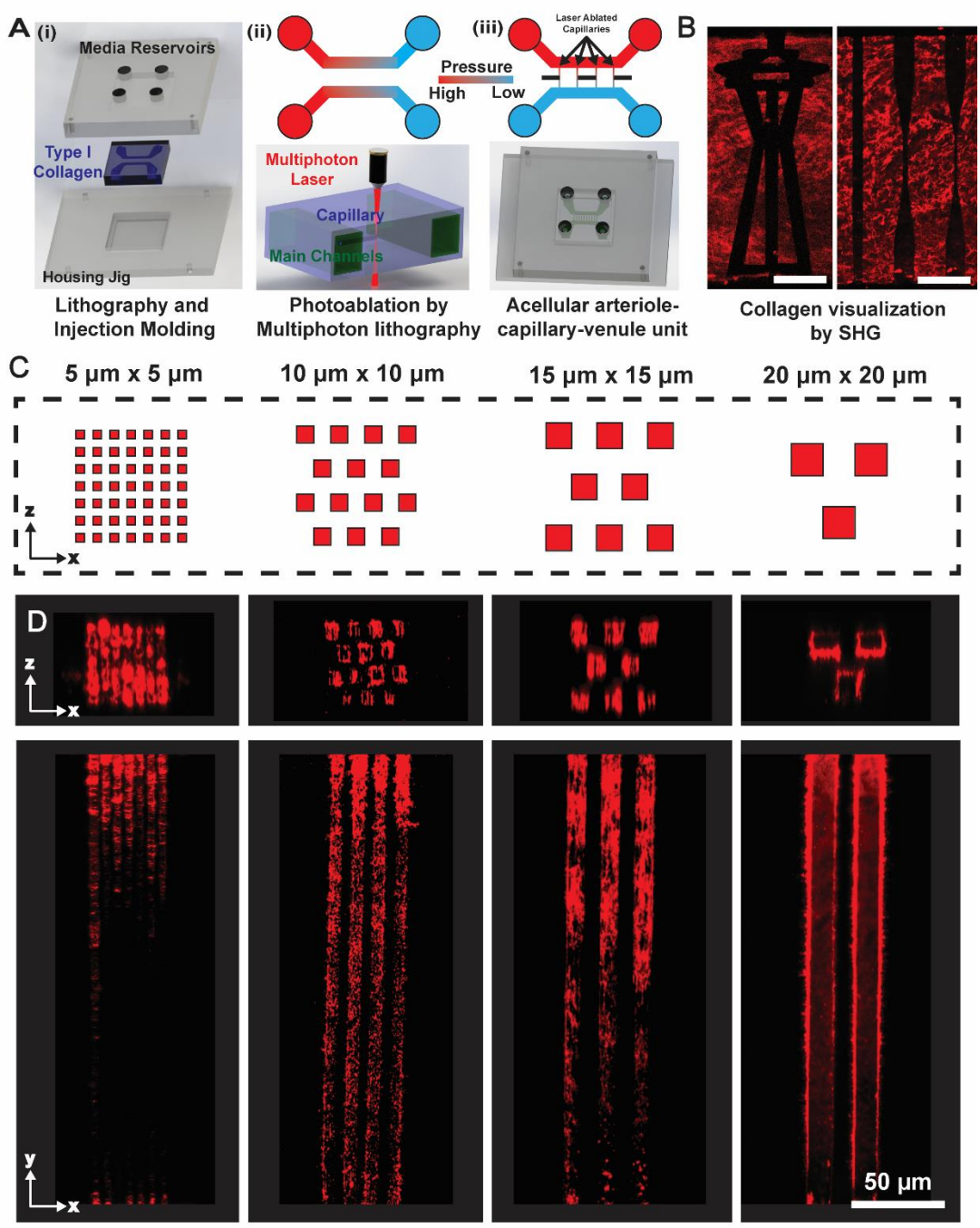

Fig. S1. Photoablation-guided fabrication of acellular capillary-sized microchannels. A. Diagram of device assembly of acellular microfluidic network in collagen via lithography and injection molding, followed by photoablation to generate void space between two microfluidic channels. **B**. Second harmonic generation (SHG) imaging of photoablated network (i.e. design of the Seattle Space Needle, left panel) and channels after photoablation. Red: collagen. Scale bar: 100 µm. **C**. Vessels ranged from 5 µm x 5 µm to 20 µm x 20 µm, where spacing and cross-sectional dimensions were made equal in size. Fluorescence beads (d = 0.22 µm) was perfused to

determine the fabrication limitations and perfusability of different-sized microchannels after photoablation. (Photo Credit: *Chris Arakawa, University of Washington*)

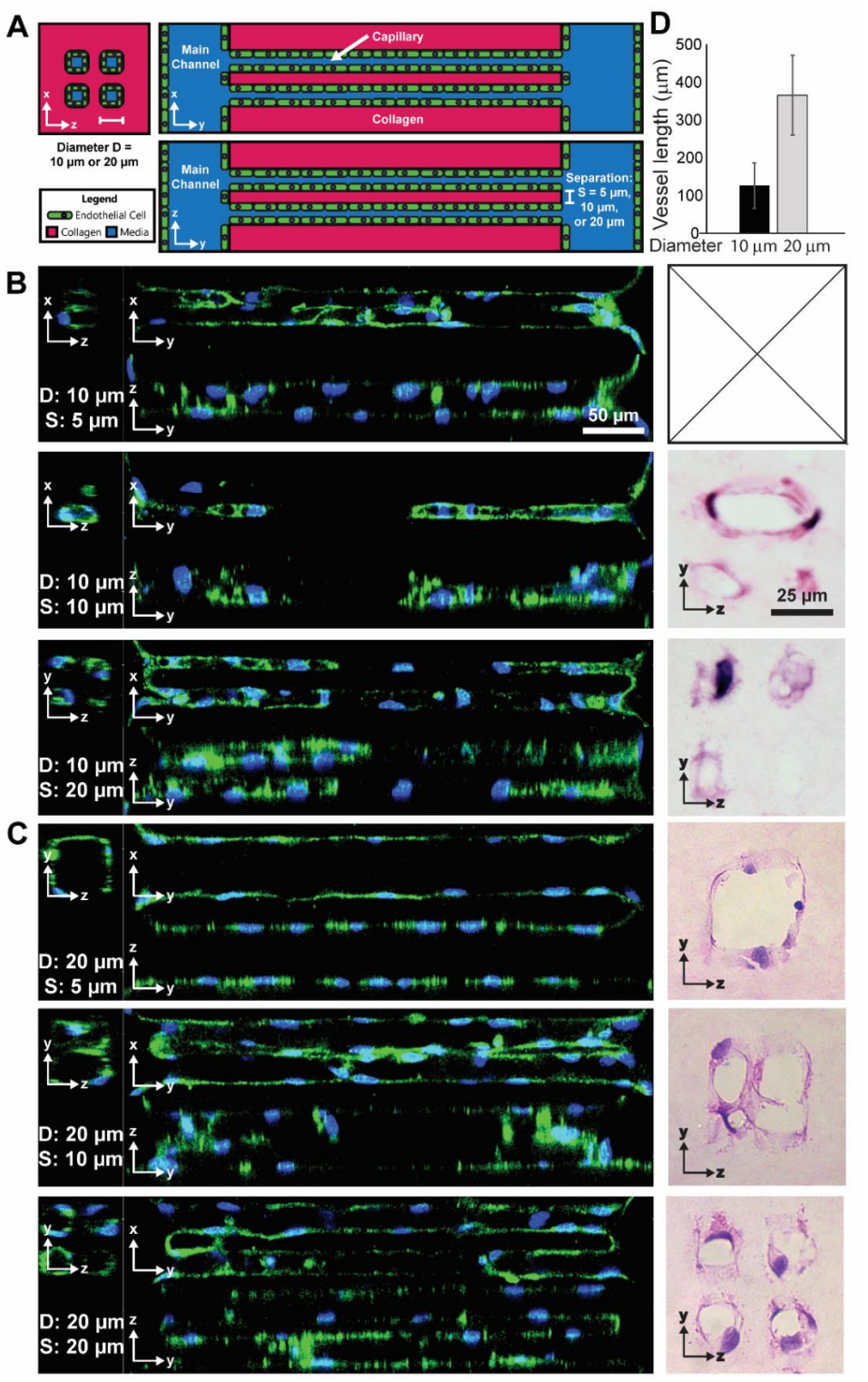

Fig. S2. Cellular limitations of capillary fabrication. As endothelial cells readily remodel their surrounding matrix, experiments were conducted to determine the size and density limitations of capillary generation over a 7-day time period. **A**. Schematic views of three cross-sectional

planes: top: X and Y dimensions (left panel) and X and Y dimensions (right panel); and bottom: Z and Y dimensions. Two main channels were pre-seeded and cultured with primary HUVECs for three days, followed by photoablation to create 2x2 arrays of either 10 μm or 20 μm diameter vessels, separated by S = 5, 10 or 20 μm to connect the two main vessels together and form ACV units. The ACV units were cultured for another 4 days (total 7 days of culture) before fixing, staining and imaging via confocal microscopy. **B-C.** Three cross-sectional views (left panels) of confocal image of 2x2 vessels arrays at diameter of either 10 μm (B) or 20 μm (C), that were separated by either 5, 10, or 20 μm, cultured for 7 days, fixed, stained, and imaged by confocal microscopy (blue = nuclei, green = von Willebrand Factor (VWF)); and right panels: H&E stained cryosections confirmed the vessel fusion when S = 5 or 10 μm, endothelial cells remodel the vessels from square to circular lumens, and incomplete cellularization when D = 10 μm. H&E images were not taken (Top right panel in B) for capillary arrays at S = 5 μm and D = 10 μm. **D.** Quantification of continuous vessel length for capillaries at diameter of 10 μm and 20 μm, measured by confocal microscopy for each ingrowth vessel into the photoablated channels spanning 450 μm in length. $p = 7.85 \times 10^{-6}$, two-tailed t-test of unequal variance. (Photo Credit: *Chris Arakawa, University of Washington*)

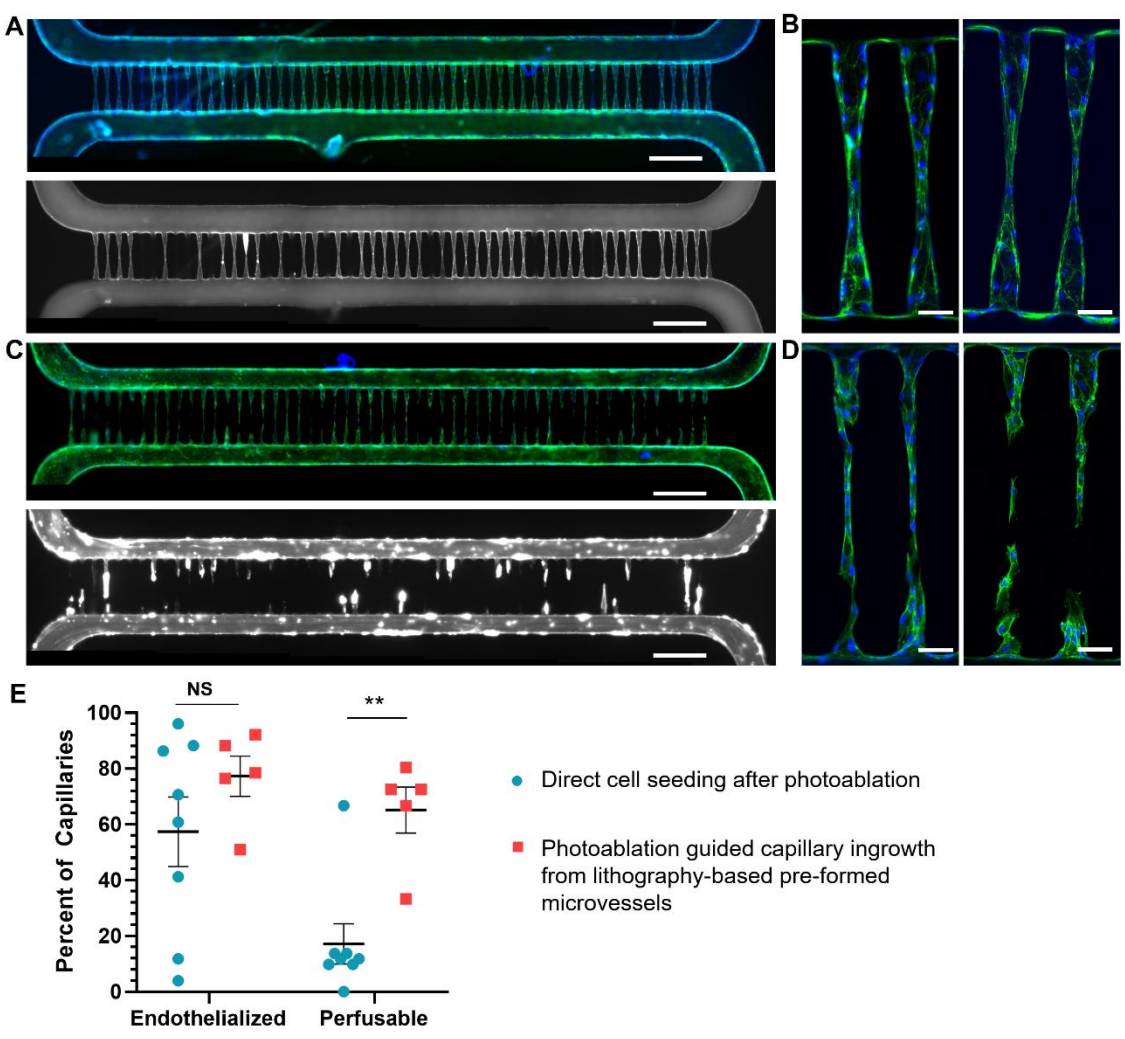

Fig. S3. Endothelialization strategies for capillary network. Two approaches were evaluated to engineer capillary-sized constriction regions across two main channels. **A-B**. Method 1: Photoablation guided endothelial cell ingrowth when performed after lithography-based microvessels are formed. A. (top) Representative images of endothelial cell staining (green: F-actin, and blue: nuclei, top panel) and (bottom) mostly perfusable vessels following a 10 min perfusion with fluorescent beads. B. Zoomed images of nearly full endothelial cell coverage in capillary-sized constriction regions between two lithographically defined microvessels. **C-D**. Method 2: Vessel formation by direct seeding into acellular collagen network with photoabalated capillary sized channels connecting between two lithographically defined ones. C. Representative images of EC staining (green: F-actin, and blue: nuclei, top panel) and non-perfusable channels with obstruction by fluorescent beads. D. Zoomed images of discontinuous

endothelial cell coverage in capillary regions between two lithographically defined microvessels. Blocked capillary constriction channels are visualized by accumulation of fluorescence clusters and incomplete channel outlines. **E**. Quantification of percent of channels that have endothelial cell ingrowth throughout the capillary-sized constriction regions or are perfusable. *: p <0.002 (two tailed t test). (Photo Credit: *Caitlin Howard, University of Washington*)

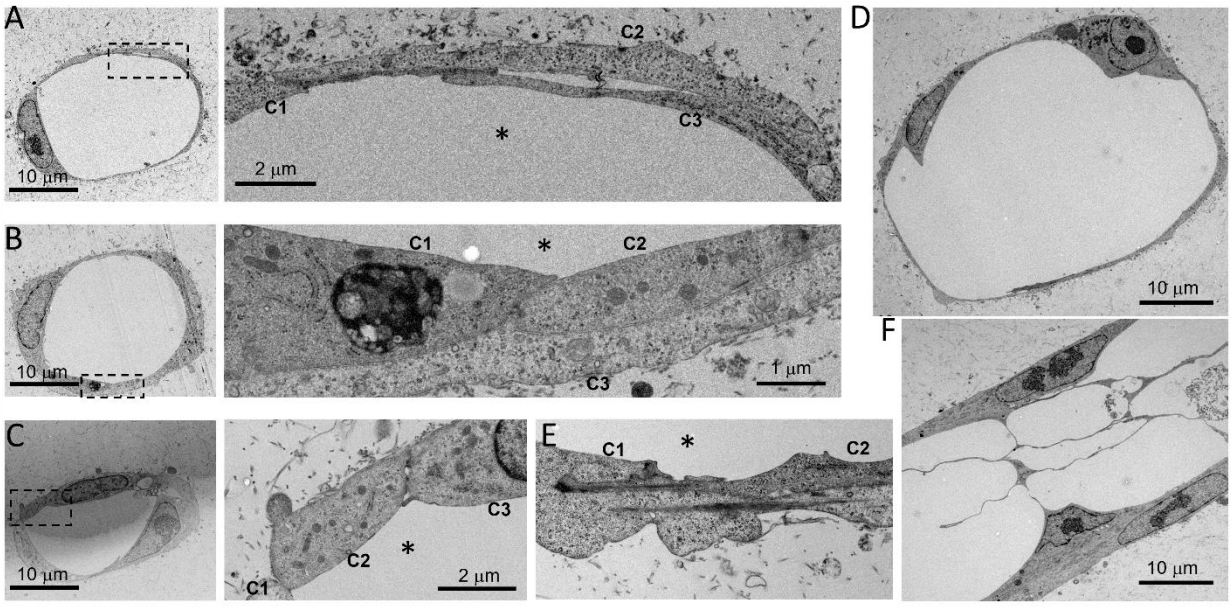

Fig. S4. Ultrastructural analysis of vessels at capillary regions across the ACV units imaged via TEM. A-D. Example cross-sectional images of capillaries at diameter of 10 – 20 μm (A-C, right panels: zoomed view of dash box in the left panels) and nearly 40 μm (D). ECs form complex junctions and focal contacts along adjacent cells to maintain vessel patency, and the lumen walls have varying thickness and diameter at different sections due to location of the cell bodies. **E-F**. Longitudinal view of ECs in capillary regions showed complex junctions (E, zoomed views) and varying diameter and height of ECs along the luminal walls (F). *: vessel lumen, C: cells. (Photo Credit: *Caitlin Howard, University of Washington*)

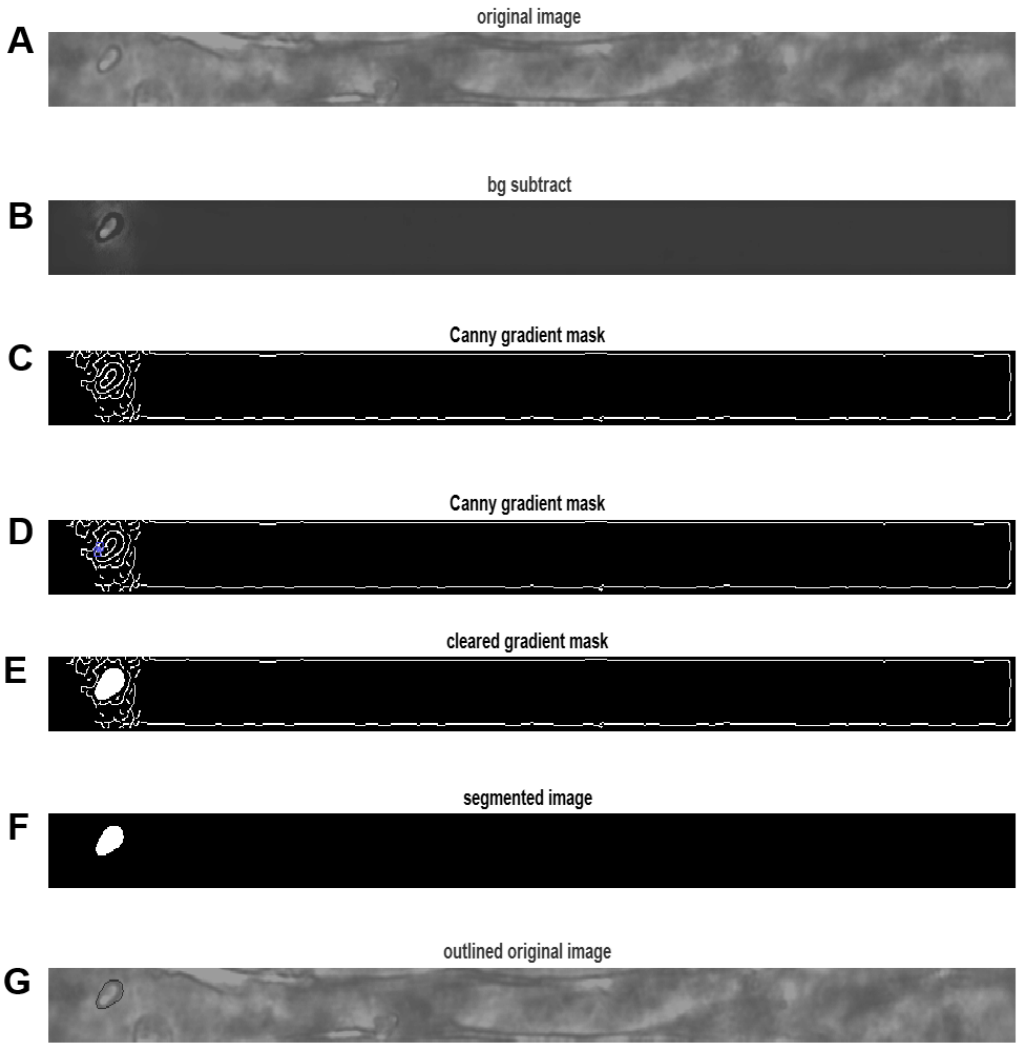

Fig. S5. Edge detection workflow for studying traversal of single RBCs through a capillary-sized constriction. To track RBCs through the engineered capillary vessels, an edge detection-based algorithm was implemented. A single frame from a brightfield video (A) was background subtracted (B) using the mean of all frames, then edge detected (C). The edge detection result was manually edited to close the contour (D), filled (E) and eroded (F) to yield a contour (G) outlining the RBC. (Photo Credit: *Celina Gunnarsson, University of Washington*)

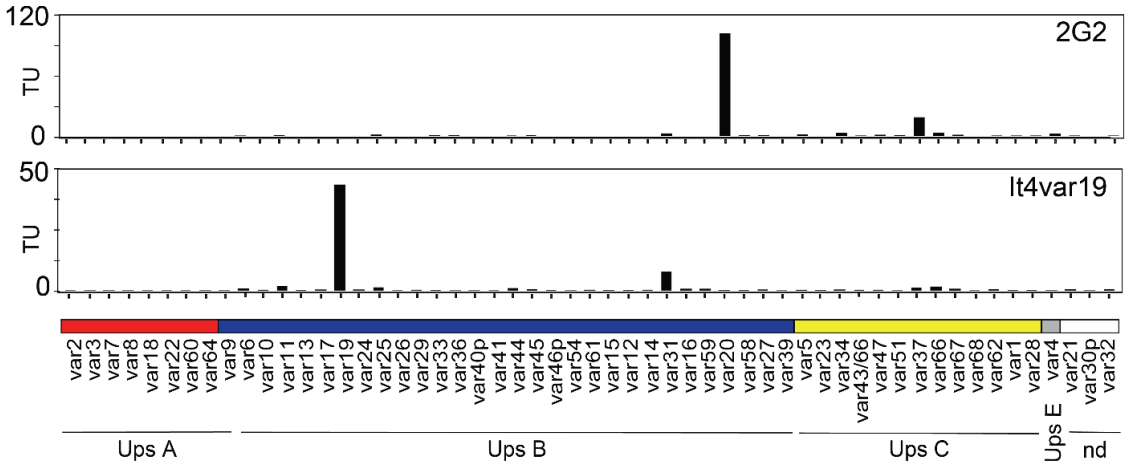

Fig. S6. Transcriptional profiling of *var* gene expression in the two parasite lines. Quantitative PCR was performed on parasite lines 2G2 and IT4VAR19 to determine *var* gene transcription profiles. Gene expression analysis demonstrates predominant expression of var20 and var19, respectively. (Photo Credit: Maria Bernabeu, *Seattle Children's Research Institute*)

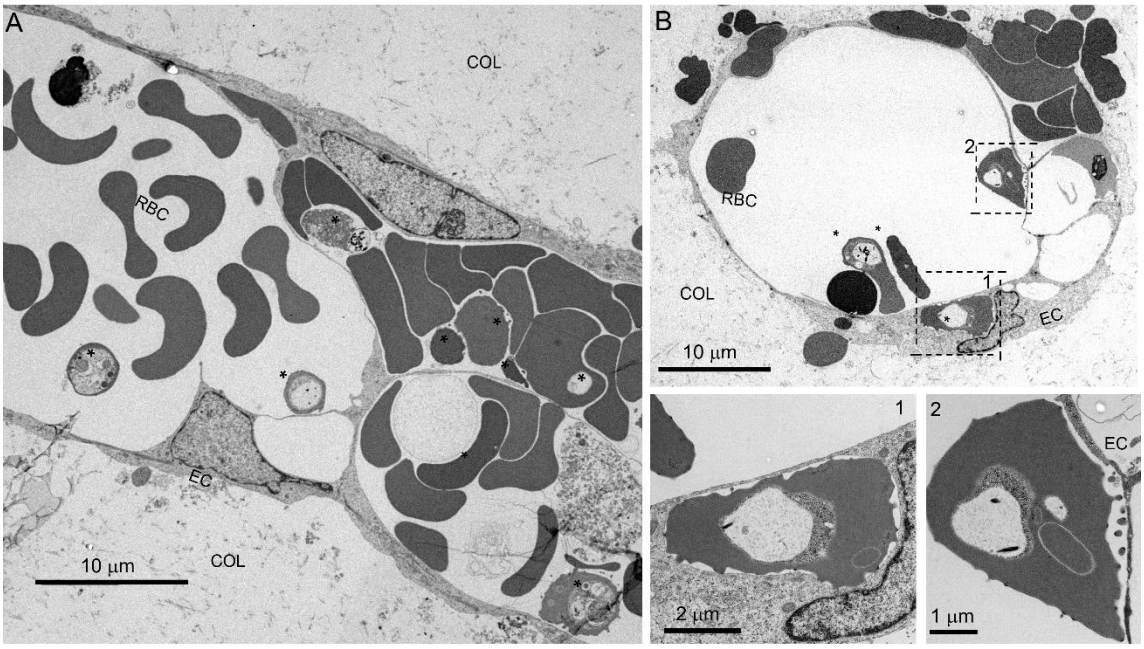

Fig. S7. Ultrastructural analysis of capillary region after perfusion of RBCs imaged via TEM. RBCs were perfused for 30 mins at physiological hematocrit (42%) with 0.5% IT4VAR19 IRBCs across the capillaries, driven by a pressure drop of 1cmH_2O. After perfusion, the vessels were washed with 1X PBS for 10 mins before fixing for TEM preparation. **A**. Longitudinal sections of capillaries with massive RBC occlusion. **B.** Cross sectional views of ACV units with IRBC adhesion after PBS washing. Bottom panels 1 and 2 are zoomed views of the dash boxes in the top panel. *: infected RBCs, COL: collagen substrate, EC: endothelial cells lining the lumen in capillary region. (Photo Credit: *Caitlin Howard, University of Washington; and* Maria Bernabeu, *Seattle Children's Research Institute*)

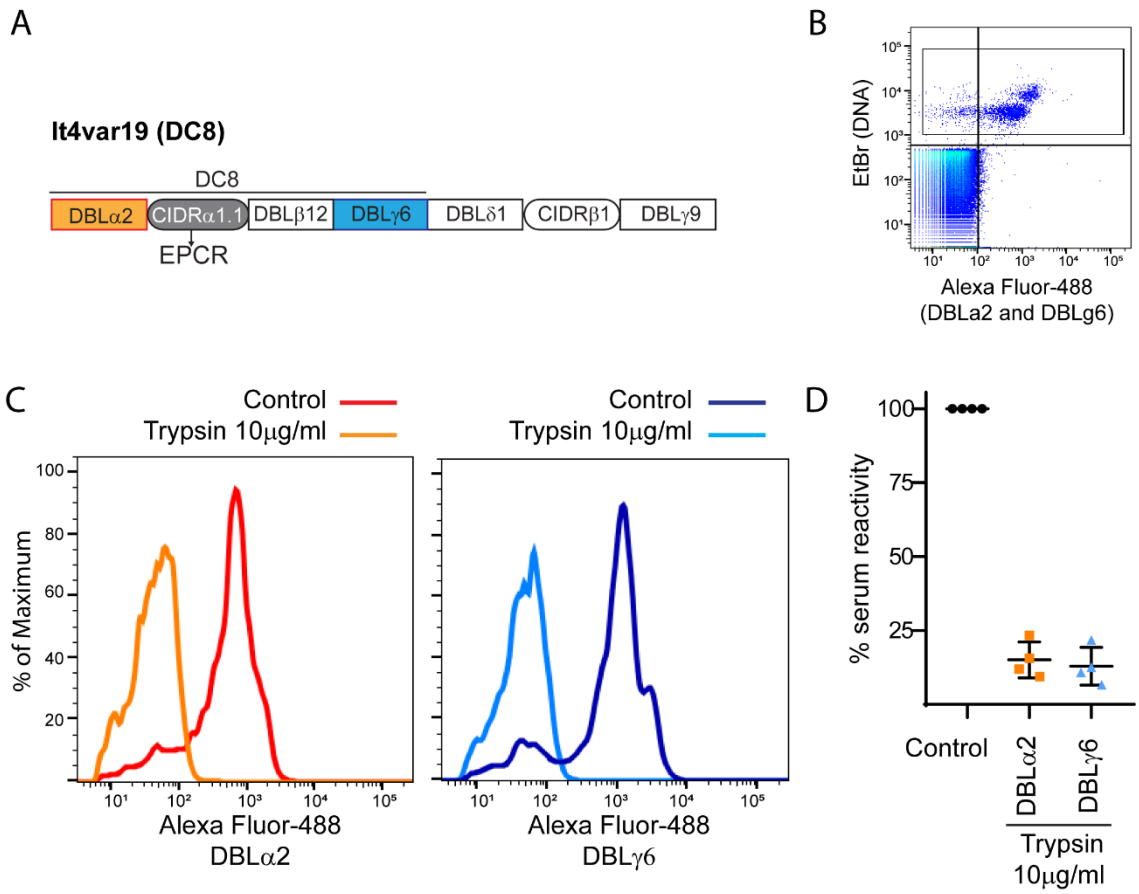

Fig. S8. Trypsin cleaves the surface-expressed IT4VAR19 PfEMP1 variant. A. Schematic of the extracellular domain architecture of IT4VAR19. Rat polyclonal anti serum was generated to the DBLα2 and DBLγ6 domains that flank the EPCR-binding CIDRα1.1 domain and was employed to study loss of antibody reactivity after IRBC trypsinization. **B.** Gating strategy for identifying surface PfEMP1 expression on IRBC. Dual labeling with ethidium bromide (EtBr) staining of parasite nuclei and a rat anti-DBLα2 or anti-DBLγ6 anti-serum was used. **C.** Representative histograms of the DBLα2 and DBLγ6 antibody surface reactivity on untreated and 10 μg/ml trypsin-treated IRBC. The EtBr-positive population of *P. falciparum*-IRBCs from panel B was gated to determine anti-DBL reactivity. **D.** DBLα2 and DBLγ6 surface reactivity on trypsin-treated IRBC relative to untreated IRBC (n = 4 independent experiments). (Photo Credit: Maria Bernabeu, *Seattle Children's Research Institute*)

SUPPLEMENTARY MOVIES:

Movie S1. Endothelial ingrowth into 20-µm capillaries between two large vessels after photoablation.

Movie S2. Representative video of normal RBCs perfused through endothelialized capillaries at physiological hematocrit.

Movie S3. Representative video of normal RBCs perfused through acellular collagen capillary-shaped channels at physiological hematocrit accumulating a significant amount before entering the capillary region and jetting and leading to significantly lower hematocrit into the downstream.

Movie S4. Representative video of normal RBCs stretching through capillaries (diameter, ~10 µm) when perfused at the single-cell scale.

Movie S5. Representative video of normal RBCs tumbling through capillaries (diameter, ~10 µm) when perfused at the single-cell scale.

Movie S6. Representative video of 2G2 IRBCs tumbling through capillaries (diameter, ~10 µm) when perfused at the single-cell scale.

Movie S7. Representative video of normal RBCs perfused through the capillaries at physiological hematocrit with no cell accumulation in the lumen.

Movie S8. Representative video of IT4VAR19 IRBCs perfused through the capillaries at physiological hematocrit accumulating a significant amount and blocking the capillary flow.

Movie S9. Representative video of trypsinized IT4VAR19 perfused through the capillaries showing a significant decrease in cell accumulation and not blocking the capillary flow.

Movie S10. Representative video of 2G2 IRBCs perfused through the capillaries at physiological hematocrit accumulating at postcapillary regions but not blocking the capillary flow.